Stability Analysis of the Synchronous Solution in Arrays of Memristive Chua's Circuits

Matteo Lodi, *Member, IEEE*, Mauro Forti, and Marco Storace, *Senior Member, IEEE*

***Abstract*—This brief studies synchronization in an array of diffusively-coupled identical memristor Chua's circuits (MCCs) with Dirichlet's boundary conditions. We start from the description of MCCs in the flux-charge domain and the state space decomposition in invariant manifolds and then we apply three different techniques, of numerical and analytic nature, for finding the synchronization condition in terms of a circuit parameter. Two of these techniques provide conditions to guarantee synchronization on any manifold and for any attractor on a manifold, while a third technique allows analyzing synchronization for each specific attractor on a fixed manifold through more precise conditions. The pros and cons of the three techniques are discussed and an application to a more realistic memristor model is provided.**

***Index Terms*—Chua's circuit, memristor, master stability function, synchronization.**

I. Introduction

NETWORKS of coupled systems are receiving increasing attention from the scientific community, from time to time focusing on the topology, the node dynamics, the connections, the synchronization (global or partial), or other aspects [1], [2], [3], [4], [5], [6], [7]. In [8], arrays of diffusively coupled identical memristor Chua's circuits (MCCs) with Dirichlet's boundary conditions were analyzed. By using the flux-charge analysis method [9], [10], [11], it was shown that the state space can be decomposed in infinitely many invariant manifolds, where each manifold is characterized by an index depending upon the initial conditions in the voltage-current domain. On the manifold with index 0, the dynamics are analogous to that of a memristor-less array of Chua's circuits, while on a manifold with an index different from 0, we obtain the dynamics of an array of forced Chua's circuits with a forcing term depending on the index. Therefore, MCCs display an extremely rich dynamical scenario where, by changing the index (i.e., the initial conditions), different types of attractors (equilibrium points, limit cycles, chaotic attractors, etc.) and even multiple attractors for a given manifold [12] can coexist.

The analysis carried out in [8] is a first step in the understanding of complex phenomena displayed by MCCs. Yet, in that paper synchronization is analyzed only on the manifold with index 0 and only by numerically simulating the state equations. The main goal of this brief is to study the synchronization of MCCs also on manifolds with an index different from 0, by using techniques of both analytical and numerical nature.

The considered MCCs array is Laplacian and with diffusive connections, which ensures the existence of a minimal conductance value of the connecting resistors, beyond which the array synchronization is guaranteed. In this brief, we study synchronization conditions for an array of N diffusively-coupled identical MCCs through three different techniques, each one with its own pros and cons. The first one is the analytical technique proposed in [13], which provides a (sufficient) condition ensuring synchronization for any attractor on any manifold. The second one is a numerical method, based on the master stability function approach [14], which provides the synchronization condition for each attractor on each manifold. The third technique is a mixed analytic/numerical method, which generalizes the technique proposed in [13] to provide a (sufficient) condition ensuring synchronization for each specific attractor on a given manifold.

The results, obtained for $N = 4$, show that all conditions are easily scalable to arrays with a generic number N of MCCs and allow us to discuss the strengths and weaknesses of each technique. Moreover, we show via an example that the methods can be applied also to circuits containing more realistic memristor models.

II. Array of Memristor Chua's Circuits

We analyze the global synchronization in a 1D array of N diffusively-coupled identical memristor Chua's circuits (MCCs). Each MCC (Fig. 1, black lines) is obtained from the well-known Chua's circuit [15], by replacing the nonlinear locally-active resistor (Chua's diode) with an ideal locally-active flux-controlled memristor, whose constitutive relation is $q = f(\varphi)$, where φ and q are the memristor flux and charge, respectively [16].

The state equations (SEs) in the (v, i)–domain of the MCCs array are $(j = 1, \ldots, N)$

$$C_1 \frac{dv_{1,j}}{dt} = -\frac{1}{R}(v_{1,j} - v_{2,j}) - \left.\frac{df}{d\varphi}\right|_{\varphi=\varphi_j} v_{1,j}$$

Manuscript received 9 February 2023; revised 3 March 2023; accepted 15 March 2023. Date of publication 20 March 2023; date of current version 12 May 2023. This brief was recommended by Associate Editor Y. Zhu. *(Corresponding author: Matteo Lodi.)*

Matteo Lodi and Marco Storace are with the Department of Electrical, Electronic, Telecommunications Engineering and Naval Architecture, University of Genoa, 16145 Genova, Italy (e-mail: matteo.lodi@unige.it; marco.storace@unige.it).

Mauro Forti is with the Dipartimento di Ingegneria dell'Informazione e Scienze Matematiche, University of Siena, 53100 Siena, Italy (e-mail: forti@diism.unisi.it).

Color versions of one or more figures in this article are available at https://doi.org/10.1109/TCSII.2023.3259008.

Digital Object Identifier 10.1109/TCSII.2023.3259008

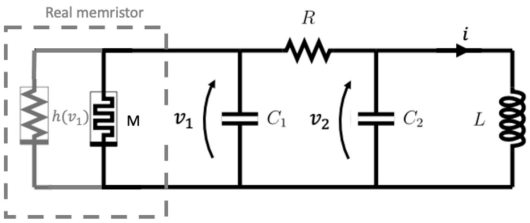

Fig. 1. Memristor Chua's circuit: original version (black) and version with a more realistic memristor model (black and gray).

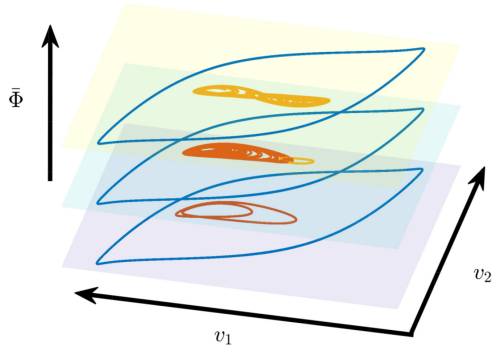

Fig. 2. Three invariant manifolds for the j-th MCC (we omit the index j) in the projection (v_1, v_2) of the state space. Each plotted manifold admits multiple attractors: the top one admits a limit cycle (blue) and a chaotic attractor (yellow), the middle one two limit cycles (blue and yellow) and a chaotic attractor (red), the bottom one two limit cycles (blue and red).

$$+\sum_{k=1}^{N}\frac{1}{R_{jk}}(v_{j,k}-v_{1,j}) \tag{1a}$$

$$C_2\frac{dv_{2,j}}{dt}=-\frac{1}{R}(v_{2,j}-v_{1,j})-i_j \tag{1b}$$

$$L\frac{di_j}{dt}=v_{2,j} \tag{1c}$$

$$\frac{d\varphi_j}{dt}=v_{1,j}$$

$$v_{1,j}(0)=v_{1,j0}\qquad v_{2,j}(0)=v_{2,j0}$$

$$i_j(0)=i_{j0}\qquad \varphi_j(0)=\varphi_{j0}, \tag{1d}$$

where R_{jk} denotes the resistor connecting the $j-$th and $k-$th MCCs through capacitors $C_{1,j}$ and $C_{1,k}$. These resistors have the same value $R_{jk}=\gamma\rho$, with $\gamma=1$ if $|j-k|=1$ and $\gamma=0$ otherwise. We also assume boundary conditions of Dirichlet type, i.e., $v_{1,0}=v_{1,N+1}=0$.

The state vector in the (v,i)-domain is $\chi=(v_{1,1},v_{2,1},i_1,\varphi_1,\ldots,v_{1,N},v_{2,N},i_N,\varphi_N)^T\in\mathbb{R}^{4N}$. According to [8], Eq. (1) admits ∞^N invariant manifolds $M(\bar{\Phi})=\{\chi\in\mathbb{R}^{4N}:\Phi_j(\chi)=\bar{\Phi}_j, j=1,2,\ldots,N\}$, where

$$\Phi_j(\chi):\mathbb{R}^{4N}\to\mathbb{R}=Rf(\varphi_j)+\varphi_j+RC_1v_{1,j}-Li_j-\sum_{k=1}^{N}\frac{R}{R_{jk}}(\varphi_k-\varphi_j).$$

Note that (i) each invariant manifold is uniquely identified by $[\bar{\Phi}_1,\ldots,\bar{\Phi}_N]\in\mathbb{R}^N$ and (ii) each trajectory must lie on one and only one invariant manifold, as illustrated in Fig. 2. We remark that each invariant manifold is nonlinear, but in the considered projection of the state space it is a hyperplane.

We then consider the MCC description in the (φ,q)-domain. By introducing the incremental flux and charge $(j=1,\ldots,N)$

$$\varphi_{1,j}(t;0)=\int_0^t v_{1,j}(\tau)d\tau,\quad \varphi_{2,j}(t;0)=\int_0^t v_{2,j}(\tau)d\tau,$$
$$q_j(t;0)=\int_0^t i_j(\tau)d\tau,\quad \varphi_j(t;0)=\int_0^t \varphi_j(\tau)d\tau,$$

we obtain the following $3N$ coupled first-order SEs in the (φ,q)-domain

$$C_1\frac{d\varphi_{1,j}(t;0)}{dt}=-\frac{1}{R}(\varphi_{1,j}(t;0)-\varphi_{2,j}(t;0))-f(\varphi_{1,j}(t;0)+\varphi_{j0})+f(\varphi_{j0})+C_1v_{1,j0} \tag{2a}$$

$$+\sum_{k=1}^{N}\frac{1}{R_{jk}}(\varphi_{1,k}(t;0)-\varphi_{1,j}(t;0)) \tag{2b}$$

$$C_2\frac{d\varphi_{2,j}(t;0)}{dt}=-\frac{1}{R}(\varphi_{2,j}(t;0)-\varphi_{1,j}(t;0))-q_j(t;0)+C_2v_{2,j0} \tag{2c}$$

$$L\frac{dq_j(t;0)}{dt}=\varphi_{2,j}(t;0)+Li_{j0}$$
$$\varphi_{1,j}(t_0;t_0)=0\quad \varphi_{2,j}(t_0;t_0)=0\quad q_j(t_0;t_0)=0. \tag{2d}$$

Let us introduce the following normalized quantities: $\alpha=C_2/C_1$, $\beta=R^2C_2/L$, $\tau=t/(RC_2)$, $\sigma=R/r$,

$$R/R_{jk}=\sigma\begin{cases}0 & \text{if } |j-k|\neq 1\\ 1 & \text{if } |j-k|=1\end{cases}=\sigma d_{jk}, \tag{3}$$

and let $n(\cdot)=Rf(\cdot)$. By using the change of variables $x_j=\varphi_j$, $y_j=Li_j$, $z_j=Li_j-\varphi_j+RC_2v_{2,j}$, we obtain the dimensionless SEs of the considered array $(j=1,\ldots,N)$:

$$\frac{d}{d\tau}\underbrace{\begin{bmatrix}x_j\\y_j\\z_j\end{bmatrix}}_{\boldsymbol{x}_j}=\underbrace{\begin{bmatrix}\alpha\Big(-x_j+y_j-n(x_j)+\Phi_{j0}\Big)\\x_j-y_j+z_j\\-\beta y_j\end{bmatrix}}_{\boldsymbol{F}(\boldsymbol{x}_j)}$$
$$+\sigma\sum_{k=1}^{N}d_{jk}\left(\underbrace{\begin{bmatrix}\alpha x_k\\0\\0\end{bmatrix}}_{\boldsymbol{H}(\boldsymbol{x}_k)}-\underbrace{\begin{bmatrix}\alpha x_j\\0\\0\end{bmatrix}}_{\boldsymbol{H}(\boldsymbol{x}_j)}\right) \tag{4}$$

where

$$\Phi_{j0}=\Phi_j(\chi(0))=n(\varphi_{j0})+\varphi_{j0}+RC_1v_{1,j0}-Li_{j0}-\sigma\sum_{k=1}^{N}d_{jk}(\varphi_{k0}-\varphi_{j0}). \tag{5}$$

If we pick the initial conditions $\chi(0)$ for the state variables in the (v,i)-domain so that we are on the 0-manifold $M(0)$, we have $\Phi_{j0}=0$ and Eqs. (4) describe an array of memristor-less Chua's circuits with a nonlinear resistor having driving-point characteristic $n(\cdot)$. By contrast, if $\chi(0)$ is such that $\Phi_0=\Phi(\chi(0))\neq 0$, the single MCC evolves on manifold $M(\Phi_0)$ and Eqs. (4) describe the same array of memristor-less Chua's

circuits, but with a non-zero constant forcing term $\alpha\Phi_{j0}$, $j = 1, \ldots, N$.

In the following, according to the treatment given in [8], we consider an ideal memristor whose flux-charge relationship is $f(\varphi) = -a\varphi + b\varphi^3$, with $a = 8/7$ and $b = 12/63$.

III. Synchronization

Our aim is to study the global synchronization of a 1D array of N diffusively–coupled identical MCCs in the (φ, q)-domain. We say that the network described by Eqs. (4) synchronizes when $\boldsymbol{x}_1(\tau) = \ldots = \boldsymbol{x}_N(\tau)$.

The synchronization of the N systems shrinks the dimension of the subspace in which the synchronous solution lies, with respect to the dimension of the full state space. This subspace is called *synchronization manifold* and is defined as $M_S = \{(\boldsymbol{x}_1, \ldots, \boldsymbol{x}_N) \in \mathbb{R}^{3N} : \boldsymbol{x}_1 = \ldots = \boldsymbol{x}_N\} \subset \mathbb{R}^{3N}$. Since the coupling is diffusive, the necessary and sufficient condition for the invariance of M_S [17] is $\Phi_{10} = \ldots = \Phi_{N0} = \bar{\Phi} \in \mathbb{R}$. This means that the isolated MCCs are identical, as they have the same constant forcing term $\alpha\Phi_{j0}$. To assess the stability of the *synchronization manifold*, i.e., to establish whether initial conditions $\boldsymbol{x}_1(0) \neq \ldots \neq \boldsymbol{x}_N(0)$ get attracted by the synchronous manifold or not, we rely on two different approaches, described in next sections, and on three related methods.

A. Analytic Conditions for Synchronization

We wish to apply the analytic results in [13] (in particular Corollary 3 and the analysis for a symmetric tridiagonal coupling) to ensure synchronization of the MCC array.

First, we have to find the minimum positive $T_1 \in \mathbb{R}$ such that the isolated MCC in the (φ, q)-domain with a negative feedback $T = \mathrm{diag}(T_1, 0, 0)$ is uniformly asymptotically stable in the sense (Yoshizawa stability) defined in [13]:

$$\begin{aligned} &\lim_{\tau\to\infty} ||\boldsymbol{x}(\tau;\boldsymbol{x}_0) - \boldsymbol{x}(\tau;\boldsymbol{x}_0')|| = 0 \\ &\dot{\boldsymbol{x}}(\tau;\boldsymbol{x}_0) = \boldsymbol{F}(\boldsymbol{x}(\tau;\boldsymbol{x}_0)) - T\boldsymbol{x}(\tau;\boldsymbol{x}_0) \\ &\dot{\boldsymbol{x}}(\tau;\boldsymbol{x}_0') = \boldsymbol{F}(\boldsymbol{x}(\tau;\boldsymbol{x}_0')) - T\boldsymbol{x}(\tau;\boldsymbol{x}_0'). \end{aligned} \tag{6}$$

According to [13], T_1 simply needs to be not smaller than the absolute value of the largest negative slope of $f(\cdot)$. Therefore, a sufficient condition on T_1 is

$$T_1 \geq a = 8/7. \tag{7}$$

From formula (26) in [13], we obtain that a sufficient condition for the array of MCCs to globally synchronize is

$$\sigma \geq \frac{T_1}{\psi(N)} = \frac{T_1}{4\sin^2\left(\frac{\pi}{2N}\right)}, \tag{8}$$

where σ is the normalized parameter introduced in Eq. (3) and $\psi(N)$ is the maximum eigenvalue of the connectivity matrix $\{d_{jk}\}$. There exist similar solutions for other topologies and, if the connections are of Laplacian type, $\psi(N) > 0$.

Remark: The sufficient conditions on T_1 and σ are independent of Φ_{j0}, namely, they *ensure synchronization for any manifold and for any attractor on a given manifold*. Actually, we expect that the conditions ensuring synchronization, which are related to the dynamics close to an attractor, depend upon both the manifold where a trajectory lies and also each attractor on a manifold, in the case of coexisting attractors; therefore, the above analytic conditions can be quite conservative.

B. Master Stability Function Approach

Note that plugging the synchronization condition $\boldsymbol{x}_1(\tau) = \ldots = \boldsymbol{x}_N(\tau) = \boldsymbol{x}_s(\tau)$ in Eqs. (4) yields $\dot{\boldsymbol{x}}_1(\tau) = \ldots = \dot{\boldsymbol{x}}_N(\tau)$. Since the N systems have the same state and the same derivative, they will follow the same *synchronized* time evolution, described by the equation

$$\dot{\boldsymbol{x}}_s(\tau) = \boldsymbol{F}(\boldsymbol{x}_s(\tau)). \tag{9}$$

Eqs. (4) can also be rewritten more compactly as

$$\begin{aligned} \dot{\boldsymbol{x}}_j &= \boldsymbol{F}(\boldsymbol{x}_j) + \sigma \sum_j d_{jk}\big(\boldsymbol{H}(\boldsymbol{x}_k) - \boldsymbol{H}(\boldsymbol{x}_j)\big) \\ &= \boldsymbol{F}(\boldsymbol{x}_j) + \sigma \sum_k a_{jk}\boldsymbol{H}(\boldsymbol{x}_k), \end{aligned} \tag{10}$$

where $A = \{a_{jk}\}$ is the Laplacian matrix, $a_{jk} = d_{jk} - \delta_{jk}\sum_k d_{jk}$, and δ_{jk} is the Kronecker's delta.

The stability analysis of the synchronous solution through the Master Stability Function (MSF) approach [14], [18] is based on the study of small perturbations $\boldsymbol{w}_j(\tau) = \boldsymbol{x}_j(\tau) - \boldsymbol{x}_s(\tau)$ about the synchronous solution, each of which evolves based on the variational equation,

$$\dot{\boldsymbol{w}}_j = D\boldsymbol{F}(\boldsymbol{x}_s)\boldsymbol{w}_j + \sigma \sum_k a_{jk} D\boldsymbol{H}(\boldsymbol{x}_s(\tau))\boldsymbol{w}_j, \tag{11}$$

for $j = 1, \ldots, N$, where D is the Jacobian operator.

Following the MSF approach, Eq. (11) can be decoupled into a number of independent blocks of the type

$$\dot{\boldsymbol{\eta}}_j = [D\boldsymbol{F}(\boldsymbol{x}_s) + \sigma\lambda_j D\boldsymbol{H}(\boldsymbol{x}_s)]\boldsymbol{\eta}_j, \tag{12}$$

$j = 1, \ldots, N$, where $\boldsymbol{\eta}_j$ is the eigenmode associated with the eigenvalue λ_j of A.

Let us introduce the MSF $\mathcal{M}(\xi)$, which associates the Maximum Lyapunov Exponent (MLE) of Eq. (12) to any possible value ξ of $\sigma\lambda_j$. We remark that only the $(N-1)$ perturbations $\boldsymbol{\eta}_2(t), \boldsymbol{\eta}_3(t), \ldots, \boldsymbol{\eta}_N(t)$ associated with the eigenvalues $\lambda_2, \lambda_3, \ldots, \lambda_N$ determine the stability of the synchronization manifold. As a result, the synchronization manifold is stable if and only if $\hat{\mathcal{M}}(\sigma) = \max_j \mathcal{M}(\sigma\lambda_j) < 0$ for $j = 2, \ldots, N$.

IV. Results

A. Bifurcation Diagram for the Isolated MCC

In this section, we analyze the possible behaviors that the isolated MCC can exhibit, by setting $\alpha = 9.5$ and $\beta = 15$. First, we define a regular grid of 40 points in the interval $\bar{\Phi} \in [0, 1]$; then we compute the brute-force bifurcation diagram by simulating Eq. (4) starting from 20 different initial conditions. Depending on the considered manifold, for a given initial condition the isolated MCC can converge to one out of three different stable attractors (one periodic and two chaotic), as depicted in the Poincaré section in Fig. 3: for $\bar{\Phi} < -0.75$ MCC can converge to the blue (periodic) and red (chaotic)

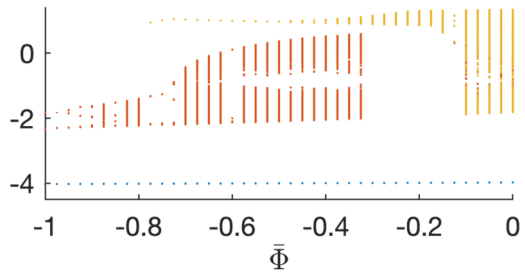

Fig. 3. Bifurcation diagram of an isolated MCC (intersections of asymptotic trajectories with a Poincaré section) vs. $\bar{\Phi}$. The circuit has up to three attractors (blue, red and yellow, with the same color code as in Fig. 2).

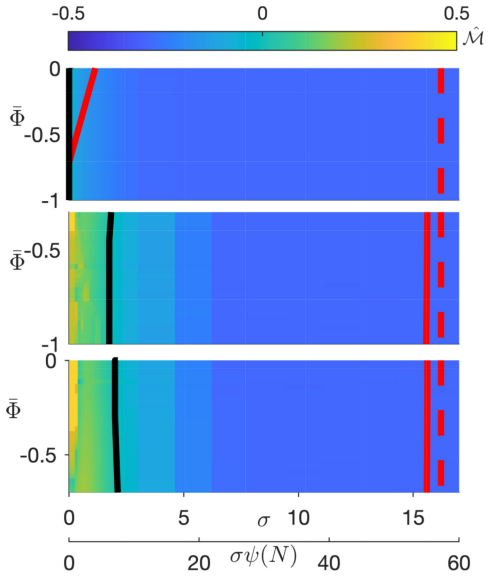

Fig. 4. Stability analysis of the synchronous solution in an array of $N = 4$ MCCs for the blue (top panel), red (middle), yellow (bottom) attractor. Stability bounds computed with method A (dashed red line), B (solid red), and C (solid black, corresponding to the zero-crossing of the MSF $\hat{\mathcal{M}}$).

attractors; for $-0.75 < \bar{\Phi} < -0.3$ MCC can converge to the blue, yellow (chaotic) and red attractors; for $\bar{\Phi} > -0.3$ MCC can converge to the blue and yellow attractors.

B. Global Synchronization in an Array of MCCs

We consider an array of $N = 4$ MCCs. To analyze the synchronization of this array, we compare three methods:

Method A – This method is purely analytic. We obtain T_1 from Eq. (7) and the stability bound of the synchronous solution from Eq. (8).

Method B – This method is semi-analytic. We obtain T_1 by solving numerically Eq. (6) and the stability bound of the synchronous solution again from Eq. (8).

Method C – This method is purely numerical. We obtain the stability bound of the synchronous solution through $\hat{\mathcal{M}}(\xi)$.

Figure 4 shows the results of this analysis with respect to the invariant set (one per panel), the manifold (through $\bar{\Phi}$), and the connection strength (through σ). The function $\hat{\mathcal{M}}(\xi)$ is color-coded as shown in the top bar: a shade of blue indicates the stability of the synchronous solution (i.e., negative MLE), whereas colors from green to yellow denote instability (i.e., positive MLE). The black line marks the stability edge obtained through method C. The dashed red vertical lines mark the sufficient condition obtained with method A. Notice that the condition is the same for any invariant set. The solid red lines mark the condition obtained with method B. Notice that, since the MSF grows monotonically with σ, the stability is determined only by the maximum eigenvalue $\psi(N)$ of the connectivity matrix. For this reason, for $N \neq 4$ we get a similar diagram with a re-scaled x-axis, as shown in the bottom part of Fig. 4.

C. More Realistic Memristor Model

The proposed techniques can also be applied to more realistic memristor circuits. Here, we briefly discuss the relevant case where the ideal memristor is replaced by a real extended memristor [11] given by the parallel connection of an ideal flux-controlled memristor and a diode-like voltage-controlled nonlinear resistor $i = h(v)$ [17] (see the gray part of Fig. 1), where the latter accounts for the rectification effect in the off-state due to the Schottky-like transport at one of the metal/oxide memristor interfaces [19]. The MCC with the new memristor model (called real-MCC) is shown in Fig. 1.

The first SE in the (v, i)-domain changes accordingly:

$$C_1 \frac{dv_{1,j}}{dt} = -\frac{1}{R}(v_{1,j} - v_{2,j}) - \left.\frac{df}{d\varphi}\right|_{\varphi=\varphi_j} v_{1,j} - h(v_{1,j}) + \sum_{k=1}^{N} \frac{1}{R_{jk}}(v_{j,k} - v_{1,j})$$

where, to fix ideas, we let $h(v) = I_S(\exp(\frac{v}{\eta V_T}) - 1)$, $I_S = 10^{-12}A$, $V_T = 26 \cdot 10^{-3}V$ and $\eta = 1.7$. The isolated oscillator is multistable, therefore its state can converge to an attractor that depends on the initial conditions. Notice that $T_1 = a$ is still a stability boundary (method A) for the more realistic memristor model, even if largely conservative. This can be easily verified owing to the passivity of the added nonlinear resistor. We apply the proposed methods to an array of $N = 4$ real-MCCs; in particular, we analyze the stability of two attractors: a chaotic attractor (top panels of Fig. 5) and a 4-cycle, i.e., a limit cycle with four oscillations per period (bottom panels of Fig. 5). The right panels show $\hat{\mathcal{M}}$ (blue curve) and the edge of stability computed with method A (dashed red line), method B (solid red), and method C (black) for the two considered attractors. We remark that this diagram holds for any N. It is apparent that also in this case method C provides the tightest condition, at the cost of a higher computational cost, as better discussed below.

V. Concluding Remarks

In this brief, we have provided a stability analysis of the synchronous solution in arrays of MCCs, by comparing three methods. Method A has a negligible computational cost (less than a second in the considered examples[1]) but provides a conservative condition. It can be extended quite

[1]Computed on a 2,3 GHz i5 quad-core processor with 16GB of RAM by using MATLAB.

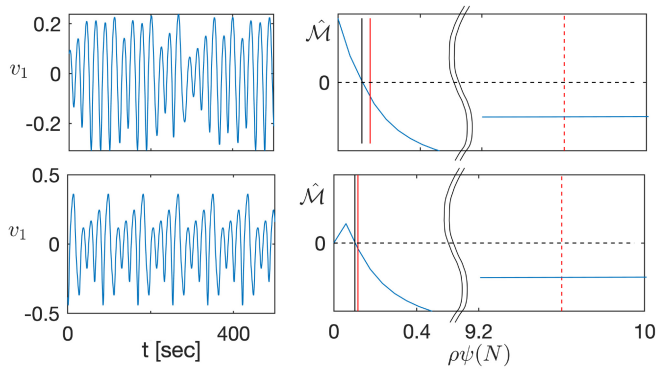

Fig. 5. Stability analysis of the synchronous solution in an array of $N = 4$ real-MCCs: chaotic (top panels) and periodic (bottom panels) synchronous solution. Right panels: $\hat{\mathcal{M}}$ (blue) and stability boundaries computed by using methods A (dashed red), B (solid red), and C (black).

easily to other network topologies but does not allow investigating separately the synchronization of different coexisting attractors. Method B is more accurate, but computationally heavier (few seconds in the considered examples[1]). Method C is the most accurate and is attractor-specific, but requires the heaviest computational effort and is network-dependent (few minutes in the considered examples[1]). The obtained results could be extended from several standpoints. First of all, other kinds of synchronization (such as cluster synchronization [20], [21], [22], [23]) can be analyzed. Second, different network topologies can be investigated, either synthetic structures (such as all-to-all, circular array, and tridiagonal structure [13]) or structures related to real applications of memristors (regular lattice, nearest neighbor, and small world [24]). Last but not least, in the MCCs we considered both an ideal flux-controlled memristor, as in the original paper by Chua [16], and a real model accounting for interface physical effects. Other more realistic models for both the memristor [11] and the other network elements (including the coupling components) would require a higher computational effort for method C and further investigations to find analytic conditions for methods A and B. As a final remark, the proposed methods provide information about *models* of real-world circuits and systems and therefore *qualitative* information about their possible behaviors. To obtain more *quantitative* information, a further step is required, i.e., to obtain experimental bifurcation diagrams, thus switching from theory to practice [25], [26], [27], [28].

REFERENCES

[1] J. J. Grainger and W. D. Stevenson, *Power Systems Analysis and Design*. New York, NY, USA: McGraw-Hill, 1994.
[2] I. Z. Kiss, Y. Zhai, and J. L. Hudson, "Emerging coherence in a population of chemical oscillators," *Science*, vol. 296, no. 5573, pp. 1676–1678, 2002.
[3] L. Stone, R. Olinky, B. Blasius, A. Huppert, and B. Cazelles, "Complex synchronization phenomena in ecological systems," in *Proc. AIP Conf.*, vol. 622, 2002, pp. 476–488.
[4] M. Rosenblum and J. Kurths, *Synchronization: A Universal Concept in Nonlinear Science*. Cambridge, U.K.: Cambridge Univ. Press, 2003.
[5] J. Shlens, F. Rieke, and E. J. Chichilnisky, "Synchronized firing in the retina," *Current Opinion Neurobiol.*, vol. 18, no. 4, pp. 396–402, 2008.
[6] L. V. Gambuzza, A. Buscarino, L. Fortuna, and M. Frasca, "Memristor-based adaptive coupling for consensus and synchronization," *IEEE Trans. Circ. Syst. I, Reg. Papers*, vol. 62, no. 4, pp. 1175–1184, Apr. 2015.
[7] R. G. Erra, J. L. P. Velazquez, and M. Rosenblum, "Neural synchronization from the perspective of non-linear dynamics," *Front. Comput. Neurosci.*, vol. 11, p. 98, Oct. 2017.
[8] F. Corinto and M. Forti, "Complex dynamics in arrays of memristor oscillators via the flux–charge method," *IEEE Trans. Circuits Syst. I, Reg. Papers*, vol. 65, no. 3, pp. 1040–1050, Mar. 2018.
[9] F. Corinto and M. Forti, "Memristor circuits: Flux–charge analysis method," *IEEE Trans. Circuits Syst. I, Reg. Papers*, vol. 63, no. 11, pp. 1997–2009, Nov. 2016.
[10] F. Corinto and M. Forti, "Memristor circuits: Pulse programming via invariant manifolds," *IEEE Trans. Circuits Syst. I, Reg. Papers*, vol. 65, no. 4, pp. 1327–1339, Apr. 2018.
[11] F. Corinto, M. Forti, and L. O. Chua, *Nonlinear Circuits and Systems With Memristors*. Cham, Switzerland: Springer, 2021.
[12] F. Corinto and M. Forti, "Memristor circuits: Bifurcations without parameters," *IEEE Trans. Circuits Syst. I, Reg. Papers*, vol. 64, no. 6, pp. 1540–1551, Jun. 2017.
[13] C. W. Wu and L. O. Chua, "Synchronization in an array of linearly coupled dynamical systems," *IEEE Trans. Circuits Syst. I, Fundam. Theory Appl.*, vol. 42, no. 8, pp. 430–447, Aug. 1995.
[14] L. M. Pecora and T. L. Carroll, "Master stability functions for synchronized coupled systems," *Phys. Rev. Lett.*, vol. 80, no. 10, p. 2109, 1998.
[15] L. O. Chua, "Global unfolding of Chua's circuit," *IEICE Trans. Fundam. Electron. Commun. Comput. Sci.*, vol. 76, no. 5, pp. 704–734, 1993.
[16] L. Chua, "Memristor-the missing circuit element," *IEEE Trans. Circuit Theory*, vol. CT-18, no. 5, pp. 507–519, Sep. 1971.
[17] F. Corinto, M. Gilli, and M. Forti, "Flux–charge description of circuits with non-volatile switching memristor devices," *IEEE Trans. Circuits Syst. II, Exp. Briefs*, vol. 65, no. 5, pp. 642–646, May 2018.
[18] L. Pecora, T. Carroll, G. Johnson, D. Mar, and K. S. Fink, "Synchronization stability in coupled oscillator arrays: Solution for arbitrary configurations," *Int. J. Bifurcation Chaos*, vol. 10, no. 2, pp. 273–290, 2000.
[19] J. J. Yang, M. D. Pickett, X. Li, D. A. A. Ohlberg, D. R. Stewart, and R. S. Williams, "Memristive switching mechanism for metal/oxide/metal nanodevices," *Nat. Nanotech.*, vol. 3, no. 7, pp. 429–433, 2008.
[20] M. Lodi, F. Sorrentino, and M. Storace, "One-way dependent clusters and stability of cluster synchronization in directed networks," *Nat. Commun.*, vol. 12, no. 1, pp. 1–13, 2021.
[21] F. Sorrentino, L. M. Pecora, A. M. Hagerstrom, T. E. Murphy, and R. Roy, "Complete characterization of the stability of cluster synchronization in complex dynamical networks," *Sci. Adv.*, vol. 2, no. 4, 2016, Art. no. e1501737.
[22] L. M. Pecora, F. Sorrentino, A. M. Hagerstrom, T. E. Murphy, and R. Roy, "Cluster synchronization and isolated desynchronization in complex networks with symmetries," *Nat. Commun.*, vol. 5, no. 1, pp. 1–8, 2014.
[23] M. Lodi, F. D. Rossa, F. Sorrentino, and M. Storace, "Analyzing synchronized clusters in neuron networks," *Sci. Rep.*, vol. 10, no. 1, pp. 1–14, 2020.
[24] T. Prodromakis and C. Toumazou, "A review on memristive devices and applications," in *Proc. 17th IEEE Int. Conf. Electron. Circuits Syst.*, 2010, pp. 934–937.
[25] O. De Feo and G. M. Maggio, "Bifurcations in the Colpitts oscillator: From theory to practice," *Int. J. Bifurcation Chaos*, vol. 13, no. 10, pp. 2917–2934, 2003.
[26] S. Valling, B. Krauskopf, T. Fordell, and Å. M. Lindberg, "Experimental bifurcation diagram of a solid state laser with optical injection," *Opt. Commun.*, vol. 271, no. 2, pp. 532–542, 2007.
[27] D. Linaro, T. Poggi, and M. Storace, "Experimental bifurcation diagram of a circuit-implemented neuron model," *Phys. Lett. A*, vol. 374, no. 45, pp. 4589–4593, 2010.
[28] Y. Kolokolov and A. Monovskaya, "Estimating the uncertainty of the behavior of a PWM power converter by analyzing a set of experimental bifurcation diagrams," *Int. J. Bifurcation Chaos*, vol. 23, no. 4, 2013, Art. no. 1350063.

Open Access funding provided by 'Università degli Studi di Genova' within the CRUI CARE Agreement